drones

Article

Accurate Estimation of Plant Water Content in Cotton Using UAV Multi-Source and Multi-Stage Data

Shuyuan Zhang [1,2], Haitao Jing [1], Jihua Dong [2], Yue Su [2], Zhengdong Hu [3], Longlong Bao [3], Shiyu Fan [3], Guldana Sarsen [3], Tao Lin [3,*] and Xiuliang Jin [2,*]

[1] School of Surveying and Land Information Engineering, Henan Polytechnic University, Jiaozuo 454000, China; 212204010003@home.hpu.edu.cn (S.Z.); jht@hpu.edu.cn (H.J.)
[2] State Key Laboratory of Crop Gene Resources and Breeding, Institute of Crop Sciences, Chinese Academy of Agricultural Sciences, Beijing 100081, China; linyuanyyds@yeah.net (J.D.); 18734672240@163.com (Y.S.)
[3] Xinjiang Cotton Technology Innovation Center, Xinjiang Key Laboratory of Cotton Genetic Improvement and Intelligent Production, Cotton Research Institute of Xinjiang Uyghur Autonomous Region Academy of Agricultural Sciences, National Cotton Engineering Technology Research Center, Urumqi 830091, China; huzhengdong1998@163.com (Z.H.); bob_ll6954@163.com (L.B.); fsy.fanshiyu@outlook.com (S.F.); gulidana2023@163.com (G.S.)
* Correspondence: lintao_xjau@163.com (T.L.); jinxiuliang@caas.cn (X.J.)

Abstract: Cotton (*Gossypium hirsutum* L.), as a significant economic crop, has undergone significant modernization in planting methods, and its smart irrigation management relies heavily on accurate cotton water content (CWC) estimation. Existing ground-based methods for measuring CWC are constrained by their limited scope and high monitoring costs. Although the development of unmanned aerial vehicle (UAV) technology has provided a new opportunity for large-scale CWC measurements, there remains a gap in the study of CWC estimation in cotton using multi-source and multi-stage data. In this study, we used UAV-based data, including texture features, vegetation indices, and a heat index, and applied four machine learning algorithms, i.e., partial least-squares regression (PLSR), support vector regression (SVR), random forest regression (RFR), and extreme gradient boosting (XGB), to estimate CWC. The findings demonstrate that in a single growth stage, the boll setting stage performs the best, and multi-source and multi-stage inputs can improve the accuracy of CWC estimation, with the best performance of XGB (R^2 = 0.860). Overall, this study highlights that the synergistic use of multi-source and multi-stage data can effectively improve CWC estimation in cotton, suggesting UAV-based data will lead to a brighter future for precision agriculture.

Keywords: UAV; smart agriculture; irrigation management; machine learning

Academic Editor: Yangquan Chen

Received: 11 January 2025
Revised: 14 February 2025
Accepted: 20 February 2025
Published: 22 February 2025

Citation: Zhang, S.; Jing, H.; Dong, J.; Su, Y.; Hu, Z.; Bao, L.; Fan, S.; Sarsen, G.; Lin, T.; Jin, X. Accurate Estimation of Plant Water Content in Cotton Using UAV Multi-Source and Multi-Stage Data. *Drones* **2025**, *9*, 163. https://doi.org/10.3390/drones9030163

1. Introduction

Cotton (*Gossypium hirsutum* L.), as an important economic crop, is directly affected by water resource management during its growth [1]. Cotton water content (CWC), which refers to the proportion of water to total weight in the cotton, is a key indicator for evaluating water stress. It is closely related to the process of plant growth and development, and the accurate measurement of its value is of great significance for optimizing irrigation strategies and ensuring healthy crop growth [2].

Traditional CWC measurements rely on the weighing method, which calculates the weight difference between dry and wet plant samples. Although this method can provide more accurate data, the operation process is cumbersome, time-consuming, and has irreversible destructive effects on plants, making it difficult to widely apply in large-scale agricultural monitoring [3]. With the advancement of technology, remote sensing technology has emerged in the field of crop physiological feature monitoring due to its non-contact, large-area, and rapid monitoring characteristics [4], especially in the non-destructive estimation of CWC, showing great potential. However, satellite remote sensing is limited by its relatively low spatial resolution and is inadequate in small-scale agricultural monitoring. It is also susceptible to interference by weather changes and fixed orbit revisit stages. These limitations greatly reduce the timeliness of data acquisition. In sharp contrast, unmanned aerial vehicle (UAV) remote sensing technology has rapidly emerged due to its advantages of flexibility, maneuverability, and high spatiotemporal resolution. It can accurately capture crop growth information in farmlands [5], providing a more reliable data source for CWC estimation, and is a focal area of research in agricultural remote sensing. For instance, Zhu et al. studied multispectral UAV imagery in wheat. They evaluated radiometric calibration methods and explored the impacts of light, flight altitude, and flight time on reflectance, vegetation index, and the inversion of winter wheat's AGB and LAI [6]. Similarly, Guo et al. utilized UAV hyperspectral data and random forest models to estimate potato canopy water content across multiple growth stages, achieving higher accuracy (R^2 = 0.85) [7]. In cotton-specific studies, Chen et al. developed a vegetation supply water index (VSWI) using RGB and thermal sensors, revealing strong correlations with leaf moisture under drought conditions [8]. These studies highlight the potential of UAV for agricultural applications.

Crop growth and development is a complex process that goes through multiple stages, each with its own unique physiological characteristics. Differences in these characteristics can largely affect the relationship between various remote sensing features and CWC. In previous studies, although there was no lack of attention to crop growth stages, the focus was on yield [9]. Most studies of crop water have a single stage; for example, Wang et al. observed the changes in stomatal conductance of bison grass under water stress through thermal infrared imagery from a drone to explore the relationship between the two [10]. But there are significant differences in crop response to water at different growth stages. This means that it is difficult to rely on a single stage to accurately capture the dynamics of CWC throughout the growth cycle. In view of this, in order to more comprehensively and accurately analyze the dynamics of CWC during crop growth, it is necessary to consider multi-stage data to build a more complete research system.

Spectral characteristics have long been regarded as an important basis for crop water content estimation [11]. Previous studies have shown that specific vegetation indices such as greenness and chlorophyll index are sensitive to water changes and can be effectively used for crop water estimation by using multiple hyperspectral vegetation indices to estimate various crop water indicators [12]. However, the study by Zhang et al. pointed out that the stability of spectral data is susceptible to environmental factors. During the high-water content stage of crops, spectral reflectance is especially prone to saturation, leading to a decrease in sensitivity to subtle changes in crop water [12]. To compensate for this deficiency, Pei et al. effectively improved the accuracy of crop water content estimation by introducing a combination of textural characteristics and vegetation indices [13]. The study by Zhou et al. also showed that combining vegetation indices with texture features can significantly improve the accuracy of estimating stomatal conductance in winter wheat, providing a more accurate method for diagnosing water stress in winter wheat [14]. In addition, thermal infrared characteristics have been validated as an important parameter source for estimating water content [15–17]. Due to the strong transpiration of plants with sufficient water, the surface temperature of their leaves is relatively low, so thermal infrared data can indirectly reflect the water status of crops. The comprehensive utilization of multiple types of remote sensing data for crop water estimation has become an important trend in current research [4].

Although there is a close relationship among spectral information, texture information, and thermal information and crop water, this relationship is mostly non-linear [13], which creates vast potential for the application of machine learning algorithms. Machine learning models can effectively handle non-linear features and heteroscedasticity problems in data, and perform well in agricultural remote sensing big data analysis [18]. Some scholars have used random forest algorithms to predict wetland biomass based on UAV multispectral images and achieved a high degree of accuracy with R^2 = 0.760 [19]; Foody et al. confirmed that support vector machines have an excellent performance in multi-class remote sensing image classification, especially when dealing with high-dimensional data and complex category structures [20]. However, current research on accurately estimating crop CWC based on multi-source data, integrating vegetation index, thermal index, and high-resolution image texture features, is still in the exploratory stage, and relevant results are relatively scarce. The aim of this study is to integrate multi-stage and multi-source data to estimate CWC in cotton using partial least-squares regression (PLSR), support vector regression (SVR), random forest regression (RFR), and extreme gradient boosting (XGB) methods to estimate CWC. The main research objectives are to (1) analyze the optimal estimation characteristics and underlying mechanisms of cotton at different growth stages, and then determine the optimal estimation parameter combination for each growth stage; (2) evaluate the performance differences of different machine learning models in CWC estimation tasks; and (3) explore the advantages of multi-source and multi-stage data compared to single-growth-stage and single-source data in estimating cotton CWC. Overall, this study is expected to provide a technological framework for smart irrigation and to help farmers apply efficient water management strategies at the best time.

2. Materials and Methods

2.1. Study Area

The study site is located at the Avati Cotton Research Station, Xinjiang Academy of Agricultural Sciences (40°27′ N, 80°21′ E) (Figure 1). This region is the core cotton production area in China, and the production model is widely represented. It has a warm temperate continental arid climate, with an annual average temperature of 10.40 °C, an annual average precipitation of 46.70 mm, an annual average evaporation of 1890.70 mm, a frost-free stage of 211.00 d, and an average annual sunshine of 2679.00 h. The soil texture in the experimental area is sandy loam soil, with a field water holding capacity of 28.92%, moderate soil fertilization, and a soil pH value of 7.33. The main high-yield cultivation technique used in the local area is subsurface drip irrigation technology.

Based on previous studies and the experience of local farmers, we determined the irrigation quota and set up five irrigation treatments based on it [21]. The two-year trial was conducted from April to October 2023 and April to October 2024, and five irrigation treatments were used, W1 (2250 m^3/hm^2), W2 (3150 m^3/hm^2), W3(4050 m^3/hm^2), W4 (4950 m^3/hm^2), and W5 (5850 m^3/hm^2), with three replicates for each treatment. The planting variety was Xinluzhong 88. Other treatments were consistent with local farmers' practices. The weather variables for the cotton growing season are shown in Figure 2.

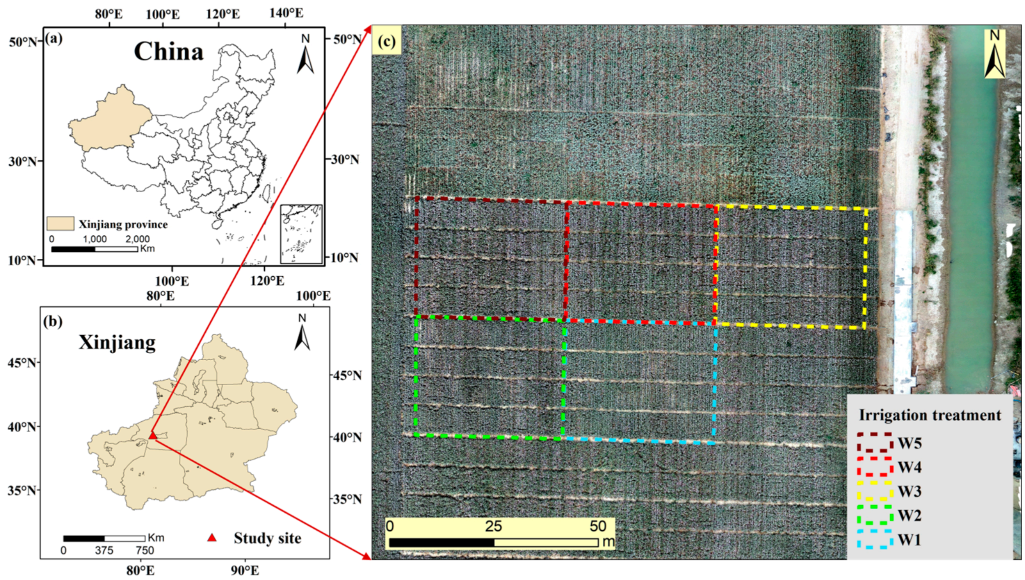

Figure 1. The general map of the study area: (**a**) a map of China; (**b**) a map of Xinjiang administrative region; (**c**) the experimental site of the study area.

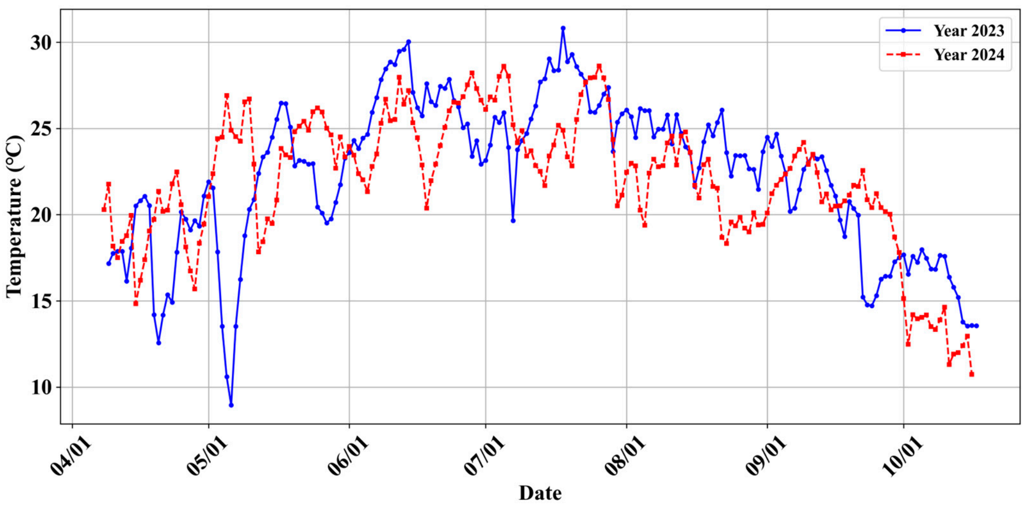

Figure 2. Temperature changes during the cotton growing season.

2.2. Data Collection

2.2.1. UAV Data Collection

This study used the DJI M210 drone equipped with a ZENMUSE XT2 red–green–blue (RGB) camera (SZ DJI Technology Co., Shenzhen, China), a ZENMUSE XT2 thermal infrared (TIR) camera (SZ DJI Technology Co., Shenzhen, China) (sensitivity of less than 50 mK), and a Micasense RedEdge MX Dual multispectral (MS) camera (MicaSense, Seattle, WA, USA) for remote sensing data acquisition (Figure 3). The UAV conducted flight operations between 13:00 and 15:00, when the sun's altitude angle was almost perpendicular to the ground. The route design task had a height of 30 m, a heading overlap rate of 75%, a lateral overlap rate of 75%, and a speed of 2 m/s and used equidistant photography with a photography interval of 2 m per image. A total of 21 flights were conducted in 2023, and 31 flights were conducted in 2024. The key growth stages (i.e., budding stage, flowering stage, boll setting stage, opening stage) for these two years were selected as 11 June 2023 (budding stage); 12 July 2023 (flowering stage); 15 August 2023 (boll setting stage); 18 September 2023 (opening stage); 13 June 2024 (budding stage); 7 July 2024 (flowering stage); 9 August 2024 (boll setting stage); and 6 September 2024 (opening stage). UAV data collection was also synchronized with each sampling event. Figure S1 provides the images acquired by three sensors.

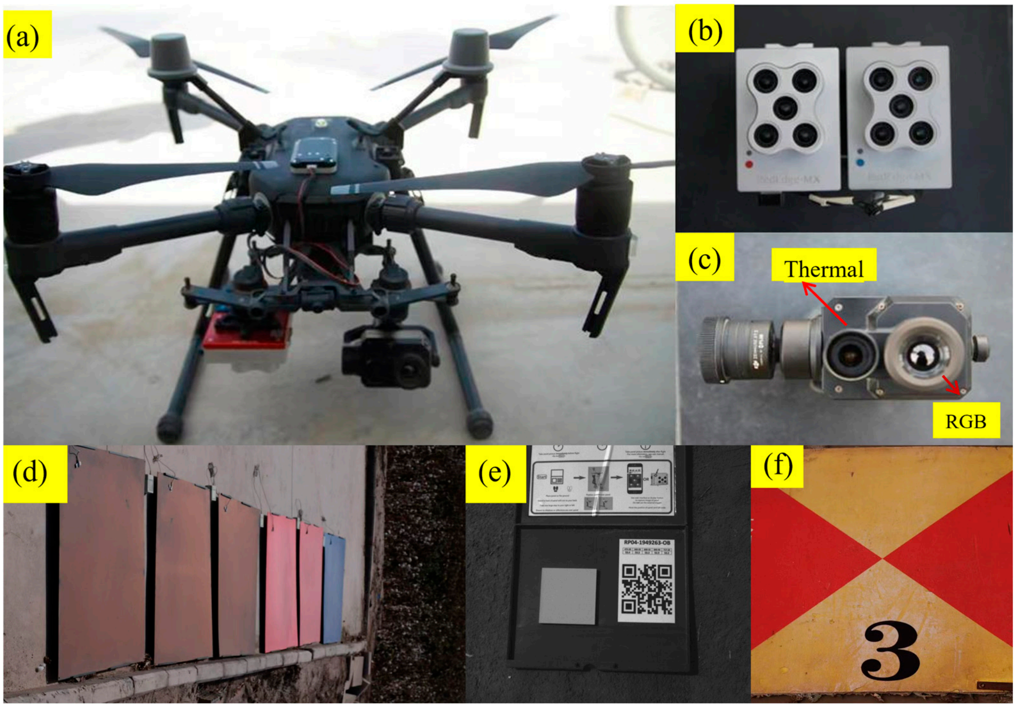

Figure 3. UAV system and corresponding devices: (**a**) DJI M210 RTK V2; (**b**) Micasense RedEdge MX dual multispectral sensors; (**c**) ZENMUSE XT2 RGB and ZENMUSE XT2 thermal infrared sensors; (**d**) temperature calibration board; (**e**) multispectral image calibration board; (**f**) ground control point.

2.2.2. CWC Data Collection

To ensure the reliability of the data and minimize errors, three cotton plants with uniform growth were randomly selected within the sampling range of each community, and their aboveground parts were taken. The water content of the cotton plants was obtained through the following steps: (1) the fresh weight (*FW*) of cotton plants was obtained; (2) the plants were put in a paper bag in an oven set at 105 °C for 30 min and then 75 °C to dry them to a constant weight; and (3) the dried weight (*DW*) of cotton was obtained and the data were recorded. Then, the average CWC of 3 cotton plants was calculated as the final value of the community. The calculation formula for CWC is as follows:

$$CWC = \frac{FW - DW}{FW} \times 100\% \tag{1}$$

In the two-year experiment, 60 valid data were obtained for each of the four key growth stages of cotton growth and development, and a total of 480 samples were obtained in the two years.

2.3. Data Preprocessing

The images obtained from multispectral and thermal sensors needed to undergo mosaic procedures, georeferencing, and calibration. We used Agisoft Metashape Professional software (version 2.1.0, AgiSoft LLC, St. Petersburg, Russia) to mosaic UAV-based images and generate corrected images. A total of 28 ground control points (GCPs) were set up in the field for geographic reference. This study used ArcGIS software (version 10.6, Environmental Systems Research Institute, Inc., Redlands, CA, USA) to perform geographic registration on the images.

After being mosaiced and georeferenced, the multispectral image and thermal image were calibrated separately. A gray board and six different colored boards set up in the field were used for the calibration (Figure 3d,e). The reflectance of the gray board for blue, green, red, red edge, and near infrared was 0.533, 0.531, 0.529, 0.528, and 0.526, respectively. To calibrate the thermal image, a temperature sensor fixed on the blackboard was applied to record the temperature of the blackboard during flight. Similarly, the relationship between the temperature of the blackboard extracted from the thermal infrared image and the digital number (DN) values was fitted as a linear function. Subsequently, this function was used to calibrate the thermal image (Figure 4).

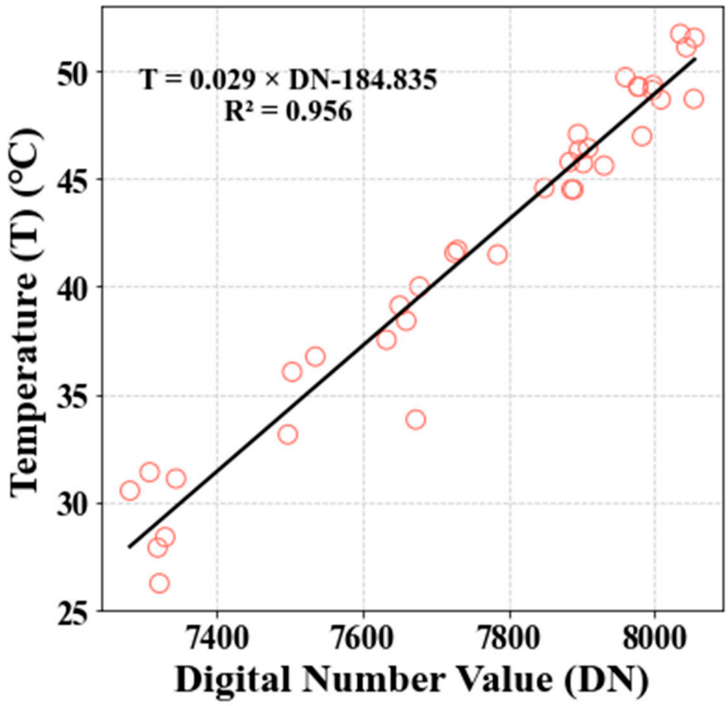

Figure 4. Conversion of DN value to temperature.

2.4. Multi-Source Features

2.4.1. Texture Features

To estimate CWC, the gray-level co-occurrence matrix (GLCM) [17], which is commonly used to extract texture feature information from UAV-based images, was employed. Eight features containing texture information were extracted based on the GLCM: variance, contrast, entropy, correlation, mean, uniformity, dissimilarity, and second moment. The RGB GLCM was obtained using ENVI software (version 5.6.0.0, Harris Geospatial Solutions, Inc., Broomfield, CO, USA). Additionally, considering the impact of resolution [18], only texture features from the red-edge (RED) and near-infrared (NIR) bands of multispectral images were extracted as supplementary information.

2.4.2. Vegetation Indices

In previous studies, the vegetation index has been used as an effective tool for estimating crop water [22]. On this basis, the CWC was estimated by calculating 19 vegetation indices using radiometrically calibrated multispectral images, as shown in Table 1. The 19 vegetation indices calculated were all input into the model as spectral information.

Table 1. The vegetation indices used in this study.

Vegetation Index	Formulation	Reference
Normalized difference vegetation index (NDVI)	$\text{NDVI} = \frac{\text{NIR}-\text{R}}{\text{NIR}+\text{R}}$	[23]
Green normalized difference vegetation index (GNDVI)	$\text{GNDVI} = \frac{\text{NIR}-\text{G}}{\text{NIR}+\text{G}}$	[24]
Optimized soil-adjusted vegetation index (OSAVI)	$\text{OSAVI} = \frac{\text{NIR}-\text{R}}{\text{NIR}+\text{R}+\text{L}}$	[25]
Soil-adjusted vegetation index (SAVI)	$\text{SAVI} = \left[\frac{\text{NIR}-\text{R}}{\text{NIR}+\text{R}+\text{L}}\right](1+\text{L})$	[26]
Modified soil-adjusted vegetation index (MSAVI)	$MSAVI = \left\{2 \times NIR + 1 - sqrt\left[(2 \times NIR + 1)^2 - 8 \times (NIR - RED)\right]\right\} / 2$	[27]
Ratio vegetation index (RVI)	$\text{RVI} = \text{NIR}/\text{R}$	[28]
Green chlorophyll index (GCI)	$\text{GCI} = (\text{NIR}/\text{G}) - 1$	[29]
Red-edge chlorophyll index (RECI)	$\text{RECI} = (\text{NIR}/\text{RE}) - 1$	[30]
Green–red vegetation index (GRVI)	$\text{GRVI} = (\text{G}-\text{R})/(\text{G}+\text{R})$	[31]
Normalized difference red edge (NDRE)	$\text{NDRE} = (\text{NIR}-\text{RE})/(\text{NIR}+\text{RE})$	[32]
Normalized difference red edge (NDREI)	$\text{NDREI} = (\text{RE}-\text{G})/(\text{RE}+\text{G})$	[29]
Simplified canopy chlorophyll content index (SCCCI)	$\text{SCCCI} = \text{NDRE}/\text{NDVI}$	[33]
The enhanced vegetation index (EVI)	$EVI = 2.5 \times (NIR - R) \;/\; (1 + NIR - 2.4R)$	[32]
Two-band enhanced vegetation index (EVI2)	$EVI2 = 2.5 \times (NIR - R) \;/\; (1 + 2.4R + NIR)$	[34]
Wide dynamic range vegetation index (WDRVI)	$WDRVI = (a \times NIR - R) \;/\; (a \times NIR + R)$	[34]
Disease water stress index (DWSI)	$\text{DWSI} = \text{G}/\text{R}$	[35]
Structure insensitive pigment index (SIPI)	$\text{SIPI} = (\text{NIR}-\text{B})/(\text{NIR}-\text{R})$	[36]
Modified simple ratio (MSR1)	$\text{MSR} = (\text{NIR}/\text{R}-1)/[(\text{NIR}/\text{R})0.5+1]$	[37]
Red-edge vegetation index (RERVI)	$\text{RERVI} = \text{NIR}/\text{RE}$	[38]

2.4.3. Thermal Index

Normalized relative canopy temperature (NRCT) is widely used to determine the water status of crops [39]. The temperature of the blackboard was recorded by a wireless temperature sensor fixed to the blackboard (Figure 3d) A linear function was fitted between this temperature and the DN value of the blackboard extracted from the thermal infrared image (Figure 4). This function was then used to calibrate the thermal image. The *NRCT* was calculated as follows:

$$NRCT = \frac{T_i - T_{min}}{T_{max} - T_{min}} \tag{2}$$

where T_i denotes the remote sensing temperature of the pixel i, and T_{min} (or T_{max}) denotes the lowest (or highest) remote sensing temperature in the whole region.

2.5. Data Integration

The data collection process was completed as described above. In this study, the normalized difference vegetation index (NDVI) was employed as the core discriminating criterion, and it was combined with the threshold segmentation method to optimize the background of remote sensing images acquired by UAVs. Due to the fact that there were insufficient data for a single stage in a year, we combined two years of data and estimated the performance of each stage as well as that of multiple stages. For the different features extracted from different images, we combined them in various ways, namely single feature, two-feature combination, and multi-feature combination, for a total of seven ways to be used as input features for the model.

2.6. Statistical Analysis

In this study, four machine learning algorithms, i.e., PLSR [40], SVR [41], RFR [42], and XGB [43], were applied to estimate CWC. PLSR can handle the problem of multicollinearity of variables. Faced with numerous correlated features extracted from multi-source remote sensing data, PLSR can explore potential variables that affect CWC, reduce feature interference, and improve estimation accuracy. Its main formula is as follows:

$$Y = \left(TP^T + E\right)B + F \tag{3}$$

where T is the latent variable matrix, P is the loadings matrix, B is the regression coefficients matrix, and E and F are the residual matrices. SVR has good generalization ability and can effectively process high-dimensional data, accurately estimate cotton water content, and is suitable for research scenarios with the combination of multiple features and complex samples. Its main formula is as follows:

$$min_{\varpi,b}\frac{1}{2}||\varpi||^2 + C\sum_{I=1}^{n}(\xi_i + \xi_i^*) \tag{4}$$

$$\begin{cases} y_i - \ \varpi^T\phi(x_i) - b \leq \epsilon + \xi_i \\ \varpi^T\phi(x) + b - \ y_i \leq \epsilon + \xi_i^* \\ \xi_i\xi_i^* \geq 0 \end{cases} \tag{5}$$

where ϵ is the insensitive bandwidth, $\xi_i\xi_i^*$ is the relaxation variable, $\phi(x)$ is the kernel function mapping, and C is the penalty coefficient. RFR has high accuracy and good anti-overfitting ability and can still stably and accurately estimate CWC in the face of complex samples and a large number of features, ensuring the reliability of estimation results. Its main formula is as follows:

$$\hat{y} = \frac{1}{K}\sum_{k=1}^{K} f_k(x) \tag{6}$$

where K is the number of decision trees, and $f_{\mathrm{k}}(\mathrm{x})$ is the predicted value of a single tree. XGB is an efficient gradient boosting framework that can capture non-linear relationships in data well and deeply explore the hidden water content changes behind the data. Its main formula is as follows:

$$\mathcal{L}(\Phi) = \sum_{i=1}^{n} l(y_i, \hat{y}_i) + \sum_{k=1}^{K}\left(\gamma T + \frac{1}{2}\lambda||\varpi||^2\right) \tag{7}$$

where l is a differentiable convex loss function that measures the difference between the prediction, $\hat{y}_i$, and the target, y_i. T is the number of leaf nodes of the tree, ϖ is the leaf weights, and γ and λ are regularization parameters.

In this study, the key parameters of the RFR, XGB, PLSR, and SVR models were confirmed by the trial-and-error approach and were optimized using the grid search method [44]. The RFR algorithm was optimized for the number of trees (n_estimators) and the maximum depth of the tree (max_depth), ranging from 100 to 300 with an interval of 50 and from 5 to 15 with an interval of 1, respectively; XGB also optimized max_depth from 1 to 10 with an interval of 1 and a subsample from 0.4 to 0.7 with an interval of 0.1; the SVR algorithm optimized the regularization parameter (C) from 0.1 to 100 and the penalty parameter (cost) from 0.1 to 0.5; PLSR optimized the max_iter of iterations from 500 to 1000 with an interval of 100; and the other parameters were left at their default values in the Python 3.11 scikit-learn package.

These machine learning algorithms have been widely used for remote sensing data estimation. To ensure a fair and comprehensive comparison of these four machine learning methods and their given input variables, this study used 70% of the randomly selected samples to train the machine learning methods and the remaining 30% to determine the accuracy of CWC estimates generated by these methods. This study applied five-fold cross-validation to verify the accuracy of the algorithms for CWC estimation. In addition, two metrics, root mean square error (RMSE) and coefficient of determination (R^2), were calculated to quantify the performance of the model. In general, the technical route of this study is shown in Figure 5.

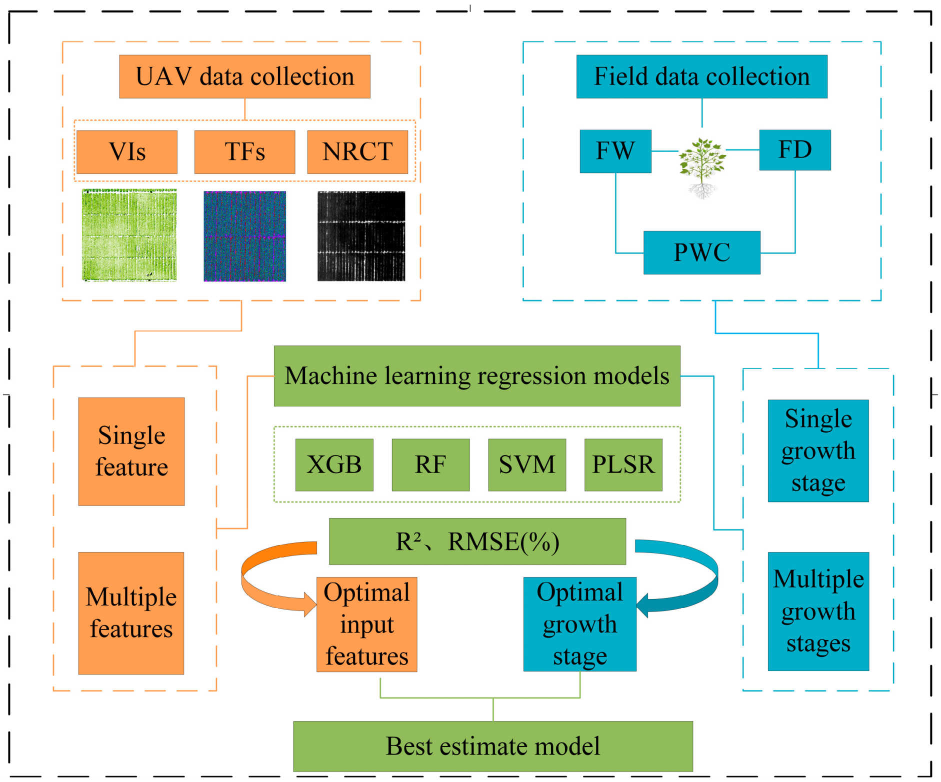

Figure 5. Technical route for estimating CWC.

2.7. Shapley Additive Explanations for Machine Learning

Shapley additive explanations (SHAP) is a technique used to explain machine learning model predictions. It originates from the Shapley value in game theory, which quantifies the impact of each feature on the final prediction result by calculating the marginal contribution of the feature to the model output. For the input sample x and model f, the SHAP value ϕ_i is given by

$$\varnothing_i = \sum_{S \subseteq F \setminus \{i\}} \frac{|S|!(|F|-|S|-1)!}{|F|!}[f(S \cup \{i\}) - f(S)] \tag{8}$$

where F is the full set of features, S is the subset of features, and $f(S)$ denotes the expected value of the model output when only the subset S is used. In this study, SHAP visualizations were generated based on the final best model. And in this way, the effect of different features on the best model for estimating cotton water content was explored, and the important factors for cotton water content estimation were found.

3. Results

3.1. Field-Measured CWC

CWC showed a decreasing trend throughout the growth stage (Figure 6). The overall variation ranged from 40.67% to 83.46%, and the distribution of data points indicated that the different treatments had a significant effect on CWC. At the early budding stage of cotton growth, CWC is at a high level. At this time, cotton is in the stage of nutrient growth; the plant grows rapidly and needs a lot of water to maintain cell division and growth and build new tissues and organs. A large amount of water is in the form of free water, so cotton in this stage has strong transpiration, thus maintaining a high CWC. As cotton enters the flowering stage, the focus of its growth is gradually shifted from nutrient growth to reproductive growth. This shift makes the water demand and distribution of cotton organs change significantly. On the one hand, the development of reproductive organs consumes a lot of energy and material, with water being an important medium for these physiological processes, playing a key role in the transportation of nutrients and maintaining cell physiological function. On the other hand, due to the change in growth mode, the efficiency of plant water utilization changes, and part of the water is preferentially allocated to reproductive organs, resulting in a decrease in overall CWC. During the boll setting stage, the growth and metabolic activities of cotton are still vigorous, and the development of cotton bolls accounts for the most water demand. The rapid expansion of cotton bolls requires sufficient water supply to ensure fiber formation and development. At the same time, the photosynthesis of the leaves, which enhances the development of cotton bolls to provide energy and a material basis, also requires water so that the physiological function of the leaves is maintained. At the boll opening stage, cotton gradually matures, the bolls begin to open and flocculate, and the fibers gradually lose water and dry out. At this time, the growth activity of cotton gradually decreases, and the demand for water is greatly reduced. Leaf photosynthesis and transpiration are also significantly weakened; part of the leaves began to senesce and shed, resulting in a further decline in the overall water content of the plant. At the same time, as cotton bolls mature, their internal water will gradually be transferred to the fibers, making the fibers dehydrated and dry, at which point harvesting and storage take place, which further reduces the CWC of the cotton plant.

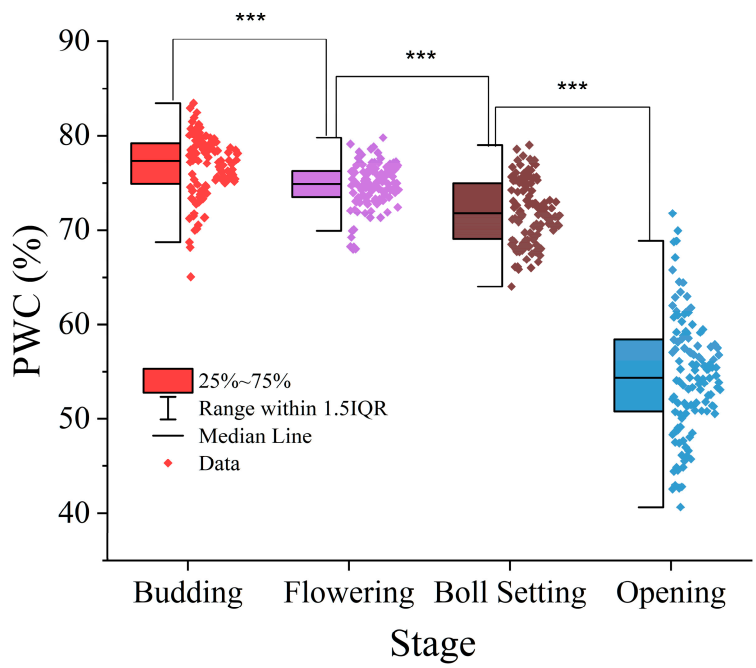

Figure 6. Distribution of CWC at different growth stages: 25% and 75% represent the upper and lower quartiles, respectively; IQR stands for interquartile range; the black line represents the upper and lower boundaries of the detected outliers. *** Represents a significant role at the level $p < 0.001$.

3.2. Dynamic Monitoring of CWC

To better analyze the effect of growth stage on CWC, we first used individual growth data to estimate CWC from spectral, textural, and thermal information from the RGB, multispectral, and thermal infrared sensors of the UAV as well as from different combinations of sensors in conjunction with the PLSR, SVR, XGB, and RFR machine learning models. The results indicated that different growth stages of cotton showed an inconsistent performance in estimating CWC. The CWC estimation was good during the budding stage (Table 2), with the highest R^2 of 0.634. At that time, the plant canopy was relatively uniform, and the vegetation index and texture characteristics performed well in reflecting the plant growth condition.

Table 2. Different machine learning models' estimations of CWC at budding stage.

Sensor Type	Feature Type *	No. of Features	Metrics	XGB	RFR	SVR	PLSR
TIR	Th	1	R^2	0.022	**0.056**	0.012	0.001
			MAE (%)	4.21%	**3.69%**	3.16%	4.21%
			RRMSE (%)	5.12%	**5.77%**	4.00%	4.97%
MS	Sp	19	R^2	0.546	**0.574**	0.552	0.544
			MAE (%)	1.87%	**1.95%**	1.89%	2.44%
			RRMSE (%)	2.73%	**2.97%**	2.97%	3.31%
RGB	Te	24	R^2	0.414	0.485	0.501	**0.504**
			MAE (%)	2.82%	2.92%	2.51%	**2.98%**
			RRMSE (%)	4.21%	4.33%	3.33%	**3.87%**
MS + TIR	Sp + Th	20	R^2	0.551	**0.580**	0.567	0.531
			MAE (%)	1.81%	**1.89%**	1.76%	2.54%
			RRMSE (%)	2.53%	**2.81%**	2.67%	3.43%
RGB + TIR	Te + Th	25	R^2	0.481	**0.548**	0.542	0.511
			MAE (%)	2.43%	**2.12%**	2.03%	2.87%
			RRMSE (%)	3.61%	**3.01%**	2.97%	3.65%
MS + RGB	Sp + Te	59	R^2	0.555	**0.596**	0.571	0.560
			MAE (%)	1.77%	**1.76%**	1.73%	2.31%
			RRMSE (%)	2.31%	**2.42%**	2.61%	3.21%
RGB + TIR + MS	Te + Th + Sp	60	R^2	0.552	**0.634**	0.584	0.561
			MAE (%)	1.79%	**1.44%**	1.64%	2.31%
			RRMSE (%)	2.48%	**2.01%**	2.45%	3.19%

Note: * Th represents the thermal index extracted from thermal infrared, Sp represents the 19 vegetation indices extracted from multispectral sensors, and Te represents the texture features extracted from RGB. Th + Sp represents the combination of spectral index and thermal index, Te + Th represents the combination of texture features and thermal index, Sp + Te represents the combination of spectral features and texture features, and Te + Th + Sp represents the combination of texture features, thermal index, and spectral features. The best result for each type of input variable is highlighted in bold.

The estimation results at the flowering stage were average and did not show as consistent a performance as in the budding stage, with R^2 = 0.491 (Table 3). At this time, the focus of cotton growth and development gradually shifted from vegetative growth to reproductive growth.

Among the four growth stages, the estimation result at the boll setting stage was the best, with an R^2 of 0.684 (Table 4). At this stage, both spectral and textural features showed significant advantages in water content estimation, but the single thermal index estimation result was not satisfactory.

The worst estimation results were obtained during the opening stage, with R^2 = 0.188 (Table 5), and the estimation results for both single- and multi-source features were unsatisfactory. This may be due to the fact that when cotton grows to the opening stage, there is an obvious senescence phenomenon of the leaves, and the physiological functions of the leaves gradually decline during this process. On the other hand, some leaves begin to fall off during the opening stage, and the canopy structure becomes less complete and uniform. This change destabilized the canopy reflectance model and made the estimation of CWC based on canopy spectral and textural features challenging. This canopy structural incompleteness also affects the acquisition and analysis of thermal infrared information, making the thermal index less accurate in reflecting the overall moisture status of cotton. However, regardless of the stage, with the combination of multi-source features, R^2 increased accordingly and performed best when all features were applied, which validated the effectiveness of multi-source data estimation of CWC. RFR performed well in all growth stages, especially in the boll setting stage (R^2 = 0.684) and budding stage (R^2 = 0.634). XGB performed generally well in a single growth stage and poorly in the flowering and opening stages. In general, SVR performed stably, while PLSR performed the worst, especially in the flowering and opening stages (R^2 = 0.013 and 0.314, respectively), with a significantly lower level of R^2 than the other models. This suggests that linear regression models struggle to handle high-dimensional, non-linear, and complex combinations of features.

Table 3. Different machine learning models' estimations of CWC at flowering stage.

Sensor Type	Feature Type *	No. of Features	Metrics	XGB	RFR	SVR	PLSR
TIR	Th	1	R^2	0.018	**0.033**	0.012	0.010
			MAE (%)	3.43%	**2.97%**	3.41%	3.21%
			RRMSE (%)	5.21%	**3.49%**	4.33%	3.97%
MS	Sp	19	R^2	0.102	0.141	**0.300**	0.214
			MAE (%)	2.99%	2.31%	**2.27%**	2.55%
			RRMSE (%)	4.39%	2.81%	**2.95%**	3.01%
RGB	Te	24	R^2	0.155	0.118	**0.258**	0.126
			MAE (%)	2.65%	2.35%	**2.35%**	2.77%
			RRMSE (%)	3.53%	2.87%	**3.11%**	3.31%
MS + TIR	Sp + Th	20	R^2	0.108	0.156	**0.382**	0.219
			MAE (%)	2.97%	2.28%	**2.16%**	2.53%
			RRMSE (%)	4.31%	2.76%	**2.74%**	2.97%
RGB + TIR	Te + Th	25	R^2	0.140	0.128	**0.369**	0.145
			MAE (%)	2.73%	2.33%	**2.21%**	2.71%
			RRMSE (%)	3.77%	2.84%	**2.87%**	3.24%
MS + RGB	Sp + Te	59	R^2	0.194	0.195	**0.483**	0.302
			MAE (%)	2.42%	2.25%	**1.85%**	2.29%
			RRMSE (%)	3.29%	2.71%	**2.35%**	2.74%
RGB + TIR + MS	Te + Th + Sp	60	R^2	0.268	0.310	**0.491**	0.314
			MAE (%)	2.27%	1.97%	**1.82%**	2.23%
			RRMSE (%)	2.80%	2.12%	**2.33%**	2.67%

Note: * Th represents the thermal index extracted from thermal infrared, Sp represents the 19 vegetation indices extracted from multispectral sensors, and Te represents the texture features extracted from RGB. Th + Sp represents the combination of spectral index and thermal index, Te + Th represents the combination of texture features and thermal index, Sp + Te represents the combination of spectral features and texture features, and Te + Th + Sp represents the combination of texture features, thermal index, and spectral features. The best result for each type of input variable is highlighted in bold.

Table 4. Different machine learning models' estimation of CWC at boll setting stage.

Sensor Type	Feature Type *	No. of Features	Metrics	XGB	RFR	SVR	PLSR
TIR	Th	1	R^2	0.016	0.010	0.019	**0.045**
			MAE (%)	3.51%	3.41%	3.21%	**3.23%**
			RRMSE (%)	4.76%	4.87%	4.77%	**4.71%**
MS	Sp	19	R^2	0.456	**0.573**	0.459	0.481
			MAE (%)	2.83%	**2.48%**	2.53%	2.83%
			RRMSE (%)	3.71%	**3.41%**	3.65%	3.91%
RGB	Te	24	R^2	0.395	**0.560**	0.385	0.505
			MAE (%)	2.92%	**2.56%**	2.77%	2.76%
			RRMSE (%)	3.97%	**3.50%**	3.89%	3.66%
MS + TIR	Sp + Th	20	R^2	0.588	**0.594**	0.517	0.501
			MAE (%)	2.52%	**2.41%**	2.40%	2.77%
			RRMSE (%)	3.07%	**3.23%**	3.10%	3.68%

Table 4. *Cont*.

Sensor Type	Feature Type *	No. of Features	Metrics	XGB	RFR	SVR	PLSR
RGB + TIR	Te + Th	25	R^2	0.523	**0.562**	0.508	0.529
			MAE (%)	2.65%	**2.55%**	2.43%	2.71%
			RRMSE (%)	3.44%	**3.49%**	3.21%	3.58%
MS + RGB	Sp + Te	59	R^2	**0.659**	0.627	0.606	0.559
			MAE (%)	**2.37%**	2.33%	2.09%	2.64%
			RRMSE (%)	**2.81%**	2.97%	2.75%	3.45%
RGB + TIR + MS	Te + Th + Sp	60	R^2	0.669	**0.684**	0.629	0.599
			MAE (%)	2.31%	**2.21%**	2.04%	2.57%
			RRMSE (%)	2.69%	**2.67%**	2.55%	3.23%

Note: * Th represents the thermal index extracted from thermal infrared, Sp represents the 19 vegetation indices extracted from multispectral sensors, and Te represents the texture features extracted from RGB. Th + Sp represents the combination of spectral index and thermal index, Te + Th represents the combination of texture features and thermal index, Sp + Te represents the combination of spectral features and texture features, and Te + Th + Sp represents the combination of texture features, thermal index, and spectral features. The best result for each type of input variable is highlighted in bold.

Table 5. Different machine learning models' estimations of CWC at opening stage.

Sensor Type	Feature Type *	No. of Features	Metrics	XGB	RFR	SVR	PLSR
TIR	Th	1	R^2	0.016	**0.020**	0.001	0.001
			MAE (%)	10.19%	**10.18%**	8.03%	9.23%
			RRMSE (%)	12.50%	**12.48%**	10.38%	11.20%
MS	Sp	19	R^2	0.032	**0.084**	0.049	0.060
			MAE (%)	9.41%	**7.74%**	8.85%	9.95%
			RRMSE (%)	11.94%	**9.51%**	11.47%	12.05%
RGB	Te	24	R^2	0.028	0.047	0.065	**0.089**
			MAE (%)	9.36%	8.56%	7.43%	**9.48%**
			RRMSE (%)	11.38%	11.37%	9.89%	**11.25%**
MS + TIR	Sp + Th	20	R^2	0.034	**0.093**	0.054	0.082
			MAE (%)	9.38%	**9.03%**	9.82%	9.39%
			RRMSE (%)	11.93%	**10.66%**	11.89%	11.77%
RGB + TIR	Te + Th	25	R^2	0.025	0.060	0.072	**0.075**
			MAE (%)	9.34%	8.41%	7.41%	**9.53%**
			RRMSE (%)	11.40%	10.81%	9.86%	**11.34%**
MS + RGB	Sp + Te	59	R^2	0.112	**1.500**	0.102	0.134
			MAE (%)	9.17%	**8.07%**	7.88%	9.66%
			RRMSE (%)	10.83%	**10.31%**	9.98%	11.73%
RGB + TIR + MS	Te + Th + Sp	60	R^2	0.125	**0.151**	0.139	0.150
			MAE (%)	9.12%	**8.03%**	7.30%	9.52%
			RRMSE (%)	10.81%	**10.23%**	9.49%	11.63%

Note: * Th represents the thermal index extracted from thermal infrared, Sp represents the 19 vegetation indices extracted from multispectral sensors, and Te represents the texture features extracted from RGB. Th + Sp represents the combination of spectral index and thermal index, Te + Th represents the combination of texture features and thermal index, Sp + Te represents the combination of spectral features and texture features, and Te + Th + Sp represents the combination of texture features, thermal index, and spectral features. The best result for each type of input variable is highlighted in bold.

3.3. Multi-Source and Multi-Growth Stage Remote Sensing Data Estimation of CWC

3.3.1. Modeling and Verification of CWC Estimation During Multiple Stages

In this study, the water content of cotton was investigated based on different growth stages, which effectively revealed the dynamic characteristics of water content at different growth stages of cotton. However, there is obvious continuity and correlation between the water content change trends of different growth stages, and only focusing on the water content change of a single growth stage may not fully reflect its dynamic characteristics. Therefore, to further analyze the dynamic changes in water content during the life cycle of cotton, we conducted a comprehensive study on the estimation of the multi-stage water content of cotton. This study demonstrated that multispectral information has a huge advantage in estimating CWC (Table 6). Of the three results estimated using a single sensor, the best results were obtained using only multispectral information, with R^2 ranging from 0.551 to 0.806. The texture features performed well, with R^2 fluctuating between 0.640 and 0.740. Thermal information extracted from thermal infrared sensors performed worse in CWC estimation compared to MS and RGB sensors, with R^2 values ranging from 0.110 to 0.205.

Table 6. Different machine learning models' results in estimating multi-stage CWC.

Sensor Type	Feature Type *	No. of Features	Metrics	XGB	RFR	SVR	PLSR
TIR	Th	1	R^2	0.185	**0.238**	0.119	0.140
			MAE (%)	9.47%	**9.14%**	10.04%	10.36%
			RRMSE (%)	12.52%	**12.45%**	14.08%	13.00%
MS	Sp	19	R^2	0.794	0.790	**0.806**	0.627
			MAE (%)	4.47%	4.89%	**4.17%**	5.87%
			RRMSE (%)	6.51%	6.71%	**5.90%**	8.35%
RGB	Te	24	R^2	0.710	**0.740**	0.647	0.655
			MAE (%)	5.04%	**4.85%**	5.08%	6.35%
			RRMSE (%)	7.13%	**6.91%**	6.96%	8.23%
MS + TIR	Sp + Th	20	R^2	0.804	0.795	**0.832**	0.634
			MAE (%)	3.93%	4.75%	**3.68%**	5.84%
			RRMSE (%)	5.72%	6.63%	**5.05%**	8.28%
RGB + TIR	Te + Th	25	R^2	0.739	**0.776**	0.774	0.659
			MAE (%)	4.95%	**4.58%**	4.21%	6.33%
			RRMSE (%)	7.05%	**6.41%**	6.31%	8.19%
MS + RGB	Sp + Te	59	R^2	**0.842**	0.836	0.842	0.774
			MAE (%)	**4.10%**	3.85%	3.69%	4.63%
			RRMSE (%)	**5.82%**	5.60%	5.56%	6.67%
RGB + TIR + MS	Te + Th + Sp	60	R^2	**0.860**	0.857	0.846	0.785
			MAE (%)	**3.58%**	3.37%	3.45%	4.41%
			RRMSE (%)	**4.94%**	5.01%	5.21%	6.50%

Note: * Th represents the thermal index extracted from thermal infrared, Sp represents the 19 vegetation indices extracted from multispectral sensors, and Te represents the texture features extracted from RGB. Th + Sp represents the combination of spectral index and thermal index, Te + Th represents the combination of texture features and thermal index, Sp + Te represents the combination of spectral features and texture features, and Te + Th + Sp represents the combination of texture features, thermal index, and spectral features. The best result for each type of input variable is highlighted in bold.

The combination of MS and RGB greatly improved the predictive power compared to using only a single sensor, with a maximum R^2 of 0.845 (XGB). The combination of RGB and TIR features showed some improvement in modeling, with R^2 ranging from 0.659 (PLSR) to 0.776 (RFR). The combination of canopy spectral, structural, and thermal information was superior to that of any combination of two sensors/features. The combination of all features derived from the three sensors achieved the best prediction with the highest R^2 of 0.860 (XGB). The performance of all models was significantly improved with this combination. This was consistent with previous results for a single growth stage and again validated the effectiveness of multi-source data combination estimation of CWC.

In the estimation of CWC over multiple stages, the performance of the XGB model gradually improved with the increase in the number of features, and it performed the best among all feature inputs; the RFR model performed similarly, and both of them were comparable in terms of overall performance; the SVR model showed relative stability; and the PLSR model performed relatively poorly under various combinations of features, and there was an obvious gap between it and the other three models. Meanwhile, it could be clearly seen that both PLSR and SVR exhibited significant overestimation and underestimation at low levels of CWC when all features were input, indicating their inadequacy in handling this particular estimation task. On the contrary, both XGB and RFR models maintained good performance in this case, performing the estimation operation accurately and showing strong adaptability and stability (Figure 7). Meanwhile, this study generated a spatial distribution map of CWC for 9 August of the 24-year period (Figure 8).

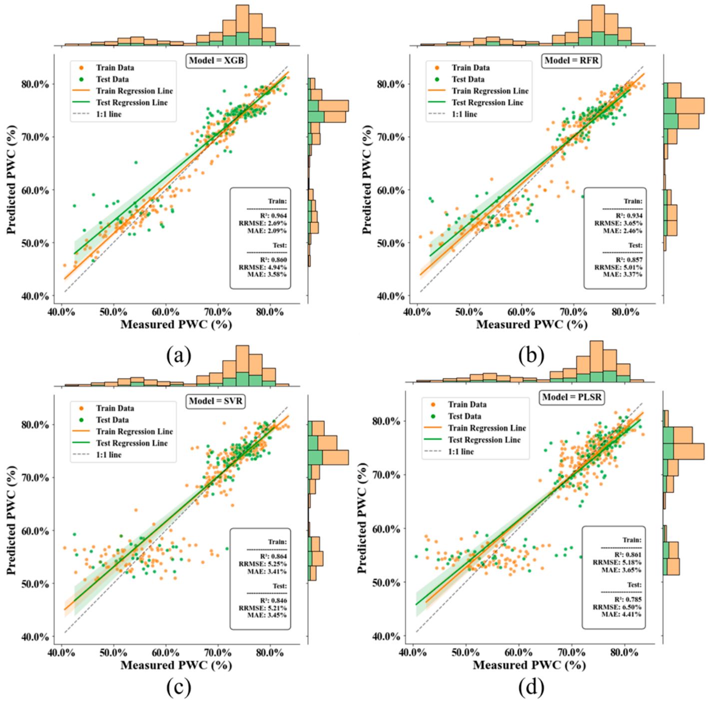

Figure 7. Performance of four machine learning models after multi-source and multi-stage data combination: (**a**) XGB; (**b**) RFR; (**c**) SVR; (**d**) PLSR. The histograms at the top and right of the figure represent the distribution of the test and training set data in measured and predicted values, where the training set is in yellow and the test set is in green.

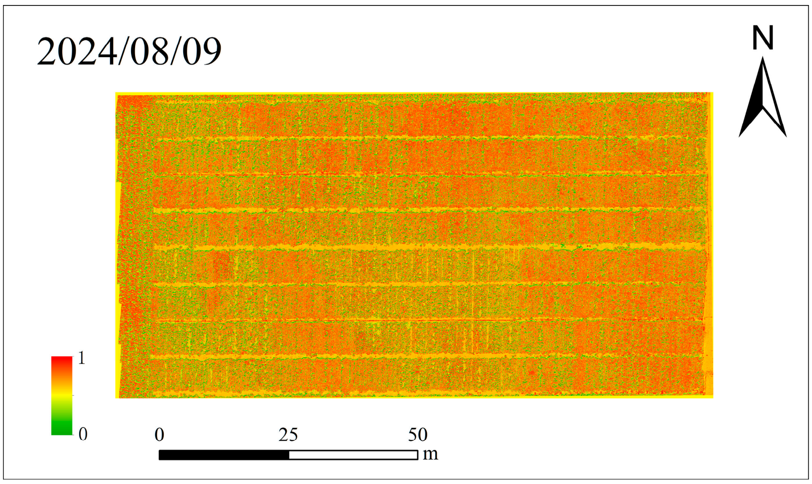

Figure 8. Spatial distribution of CWC on 9 August 2024.

3.3.2. Importance of Model Features

To assess the importance of individual features in CWC estimation, this study selected the best model (XGB) for SHAP visualization (Figure 9). Our results indicate that vegetation indices and textural features were key drivers in estimating CWC. Vegetation indices contributed significantly to the prediction model by directly characterizing plant spectral features. Textural features complemented the prediction model by capturing subtle changes in plant water stress and canopy structure. Our SHAP analysis showed that among the vegetation indices, EVI was the most contributive metric, with a wide range of SHAP values and a clear distribution of positives and negatives. Higher values of EVI contributed significantly to positive prediction, indicating that the EVI value increased significantly when water content was high. This further suggests that EVI is more suitable for describing vegetation conditions in high-humidity environments. Similarly, high values of GRVI contributed significantly positively to the model, reflecting the close relationship between vegetation activity and water content. For textural features, high values of nir_Homogeneity in the NIR band significantly and positively contributed to water content prediction, suggesting that highly correlated and uniformly distributed textural features in the canopy corresponded to healthy and high-water-content plant states. High values of metrics such as entropy and correlation (nir_Correlation, nir_Entropy) had a strong negative contribution to the model, suggesting that increased textural variability under water stress or low water content provided critical information to the model. The combination of vegetation indices and texture characteristics provided multi-source information support for the accurate estimation of cotton water content during multiple stages. In addition, the thermal index (NRCT) provided an important supplement for capturing water changes.

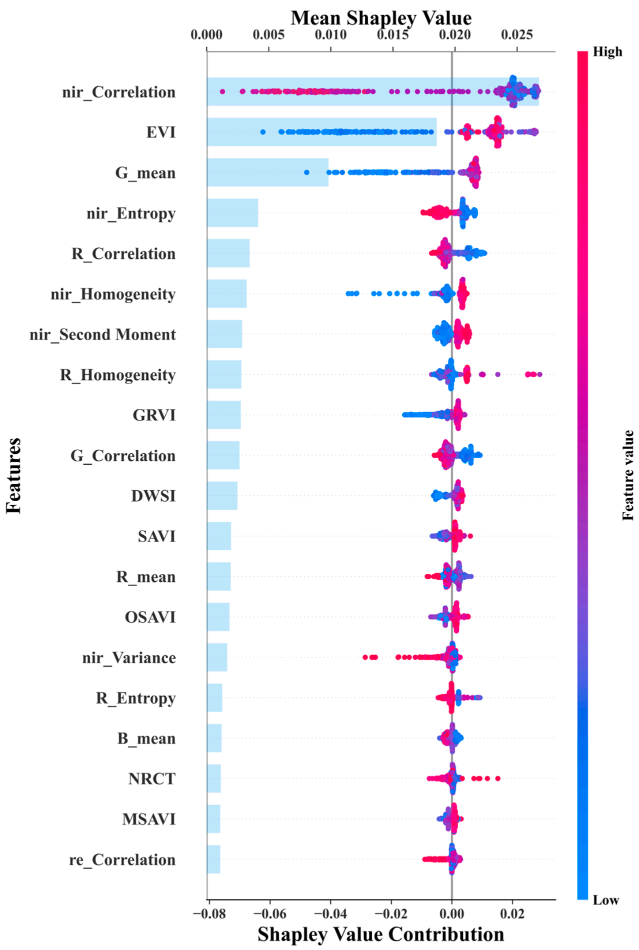

Figure 9. The model features' importance ranking and SHAP analysis.

4. Discussion

4.1. Links Between UAV Multi-Source Data and CWC

In this study, most of the variables that performed well in estimating CWC were closely related to the NIR band, which is consistent with the theory that the NIR band is a water-sensitive band [45]. Spectral features exhibited significant advantages in CWC estimation, which is consistent with numerous previous research results [11]. This study further found that the combination of RGB and multispectral information can significantly improve the estimation accuracy of CWC, possibly because texture features overcome the problem of spectral feature saturation to a certain extent [14]. Peng et al. achieved good accuracy by extracting the band reflectivity, canopy coverage, and canopy temperature of grape leaves, combined with machine learning, to predict their water content [21]. Similarly, in this study, vegetation indices, texture features, and a thermal index were calculated for estimation, and the accuracy of the estimation results was improved. This may be because vegetation indices and a thermal index can enhance signal stability, highlight physical significance, and comprehensively reflect multidimensional factors of vegetation status and environmental stress. This study utilized multi-source data, which not only consider spectral information but also incorporate texture and thermal information. Compared to data from a single sensor, it can provide more comprehensive information on plant health and water status, effectively compensating for the shortcomings of a single data source and reflecting plant water status more comprehensively. This study provided new ideas and methods for accurately estimating CWC by integrating multiple types of information.

4.2. Effects of Using UAV Single-Stage and Multi-Stage Data to Estimate CWC

This study conducted estimations of CWC during a single growth stage and multiple stages, and the results showed significant differences between the two, which have important implications. Firstly, they indicate that relying solely on single-growth-stage data may lead to inaccurate assessments of cotton's water requirements over the entire growth period. This could potentially result in either over-irrigation, which wastes water resources and may lead to other problems such as soil salinization, or under-irrigation, which can limit crop growth and yield. Secondly, the multi-stage analysis revealed the complex relationship between the growth stage and water content, suggesting that different strategies may be needed at different stages to optimize water use efficiency. Previous study by Santesteban et al. used high-resolution UAV thermal imaging for vineyard plant water status research, offering important references for understanding crop water status at different stages [15]. Regarding the multi-stage aspect, Zhou et al. found that a model combining texture features and a vegetation index had higher accuracy and stability in diagnosing winter wheat water stress through comparing different feature combinations [14]. Similarly, this study added the heat index to further enrich crop water-related information. Wang et al. constructed a robust model for winter wheat water stress diagnosis by combining UAV multispectral and thermal remote sensing data [46]. Compared with these studies, the combination of multi-source data adopted in this study more fully takes into account the various data related to water content and verifies the validity of multi-source and multi-stage data. However, according to previous research, canopy structure has a significant impact on spectral reflectance and related feature extraction [47]. Meanwhile, changes in water transport pathways and rates can weaken the correlation with UAV image features [48]. These factors collectively increase the uncertainty of CWC prediction and the difficulty of model training. When estimating CWC over multiple stages, the model faces the challenge of complex changes in different growth stages, requiring stronger generalization and feature integration abilities. Therefore, this study fully utilized the advantages of multi-source data by integrating data from multiple stages, and more comprehensively reflected the water status of cotton throughout the entire growth cycle. The estimation results of multiple stages indicated that multi-source data combination has significant advantages in capturing the dynamic changes in CWC. By integrating data from multiple stages, the model can obtain more comprehensive information, thereby more accurately reflecting the water status of cotton throughout the entire growth cycle. This result emphasizes that when conducting crop water monitoring, information from multiple stages should be comprehensively considered to improve the accuracy and reliability of estimation.

4.3. Performance Differences Among Machine Learning Models

Machine learning models have become important tools for solving non-linear problems and have shown broad potential in complex remote sensing applications. This study compared the performance of four machine learning algorithms in multiple stages and in a single growth stage and found that the XGB model performed the best in multi-stage estimation. The XGB model has significant advantages in high-dimensional and multi-source data estimation tasks due to its fast processing ability for complex samples and multidimensional features, as well as strong its anti-overfitting properties [49]. However, in the case of a single growth stage, XGB's performance was not as good as that of RFR. This may be due to the small sample size of a single growth stage and the sensitivity of XGB to data noise, which limited its adaptability to small-sample scenarios [50].

In addition, as some studies have shown, due to the non-linear relationship between water and spectral features [51], research has found that non-linear models perform better overall than linear models in CWC estimation. Multi-source data combination has significant advantages in modeling complex spectral water relationships. However, the performance improvement of PLSR in the context of multi-source data combination was limited. This could be attributed to the fact that PLSR has poor adaptability to non-linear relationships and cannot fully tap into the potential of new data, resulting in its overall effectiveness being weaker than that of non-linear algorithms. Therefore, the importance of model selection cannot be ignored in complex remote sensing data processing. This study comprehensively verified the key role of multi-source data combination and appropriate machine learning algorithm selection in improving CWC estimation accuracy through experiments, providing a more solid theoretical and practical foundation for future precision agriculture applications, and emphasizing the importance of model selection in complex remote sensing data processing.

4.4. Limitations and Future Work

Although this study achieved good results in estimating CWC through multi-source data combination, there are still many shortcomings. First, in terms of data acquisition and processing, although a variety of features were extracted from the multiple sensors carried by the UAV, the exploration of RGB and thermal infrared information was not comprehensive enough. For example, RGB only focuses on extracting texture features, while thermal infrared utilizes a limited number of thermal indices, which may miss important information contained in the structural features, the color features of RGB, and more thermal indices. And this not fully utilized information may further improve the accuracy of CWC estimation. Meanwhile, spectral information and canopy thermal information easily overlap [52], which may interfere with the model's capture of critical information, affecting the accuracy and reliability of the final estimation results and limiting the application of the research results on a wider scale. Secondly, in the selection of machine learning methods, commonly used methods were adopted in this study. Although these methods have shown a certain degree of effectiveness in previous studies and in this study, more advanced machine learning or deep learning methods continue to emerge as the field of machine learning continues to develop [53]. In contrast, existing methods may not be sufficient to deal with complex multi-source data and explore deeper features of the data, thus limiting the further improvement of the accuracy of CWC estimation, failing to give full play to the potential of multi-source data combination and making it difficult to better satisfy the increasing accuracy requirements of precision agriculture for crop water management. In future research, more advanced machine learning models, especially neural networks, may lead to better performance; however, considering the large amount of data required for deep learning, we need to actively collect more UAV data and expand the dataset size to provide sufficient data support for neural network training. At the same time, some lightweight neural network structures could be applied to reduce the computational cost and improve the scalability of the model. In addition, the method of estimating CWC using UAV multi-source data and machine learning algorithms in this study has the potential to be generalized to other crops to a certain extent, but inter-crop differences need to be considered. For common crops such as wheat and maize, some scholars have already achieved valuable results using similar remote sensing data and analysis methods. This indicates that the idea of multi-source data fusion and the model construction method in our study are somewhat generalizable. However, there are significant differences in the physiological characteristics, growth cycles, and canopy structures of different crops. For example, different leaf morphology and organization can lead to different light absorption, reflection, and transmission characteristics, which in turn affect the relationship between spectral characteristics and moisture. In addition, differences in crop growth cycles can affect the collection and analysis of multi-stage data. Some crops with short growth cycles may require more frequent data collection, while crops with long growth cycles face more complex environmental changes at different stages, requiring greater model adaptation. Therefore, when extending the results of this research to other crops, data collection schemes and models need to be appropriately adapted and optimized according to the specific characteristics of the crops. In summary, these limitations affect, to some extent, the accuracy, generalizability, and guidance of the results of this study in the practical application of precision agriculture. Future studies need to improve and refine these issues to promote the continuous development of CWC estimation research and provide better data support and a better basis for decision-making for precision agriculture practice.

5. Conclusions

This study evaluated the effectiveness of four machine learning algorithms (PLSR, SVR, RFR, and XGB) in estimating CWC by integrating multi-source and multi-stage data. The results showed that multi-source data combination significantly improved the accuracy of CWC estimation. The estimation results of multi-stage data significantly improved compared to those of single-growth-stage data. RFR performed the best in the single growth stage, while the XGB model slightly outperformed RFR in multiple stages. The present study provided a new technological approach for water resource management in precision agriculture. Through multi-source data combination and appropriate machine learning algorithms, crop water status can be monitored and managed more accurately, and irrigation strategies can be optimized to improve crop yield and quality. The successful implementation of this approach can help farmers to accurately understand the water requirements of cotton at different growth stages. This would allow them to implement precise irrigation strategies for different areas of a cotton field. On the other hand, the results of this study fully demonstrate the importance of utilizing advanced technology to achieve precision irrigation for agricultural water conservation and sustainable development. Based on these results, policy makers can promote related technologies and equipment in different regions, guide farmers to adopt precision irrigation, and promote the transformation and upgrading of agricultural production methods. At the same time, policy makers can allocate water resources more rationally according to the current situation, optimize the structure of agricultural water use, improve the overall utilization efficiency of water resources, and provide a strong guarantee for the long-term stable development of agriculture. Future research could further explore more types of remote sensing data and more advanced machine learning algorithms to further improve the accuracy and usefulness of CWC estimation.

Supplementary Materials: The following supporting information can be downloaded at: https://www.mdpi.com/article/10.3390/drones9030163/s1, Figure S1: Actual image acquired by the three sensors; Figure S2: Features extracted from three images; Figure S3: Control point accuracy for geographic alignment; Figure S4: Table 5 Scatterplot; Figure S5: Table 6 Scatterplot.

Author Contributions: Conceptualization, S.Z., T.L., and X.J.; Funding acquisition, H.J., T.L., and X.J.; Investigation, S.Z., J.D., Y.S., Z.H., L.B., S.F., and G.S.; Methodology, S.Z. T.L., and X.J.; Writing—original draft, S.Z.; Writing—review and editing, T.L., and X.J. All authors have read and agreed to the published version of the manuscript.

Funding: This work was funded by the National Cotton Industry Technology System of China (CARS-15-12); the National Key Research and Development Program of China (2024YFD2300604); the Key Research and Development Program of Xinjiang Uygur Autonomous Region (2024B02004); the Central Government Guide to Local Projects (ZYYD2024CG23); the Agricultural Science and Technology Innovation Stable Support Program of Xinjiang Academy of Agricultural Sciences (xjnkywdzc-2023007); and the Tianshan Talent Training Program (2023TSYCTD004). This research was also funded by the Nanfan special project, CAAS (YBXM2401, YBXM2402, PTXM2402), the National Natural Science Foundation of China (42471361), and the Agricultural Science and Technology Innovation Program of the Chinese Academy of Agricultural Sciences.

Data Availability Statement: The data presented in this study are available on request from the corresponding authors. The data are not publicly available due to privacy restrictions.

Conflicts of Interest: The authors declare no conflicts of interest.

References

1. Lacerda, L.N.; Snider, J.L.; Cohen, Y.; Liakos, V.; Gobbo, S.; Vellidis, G. Using UAV-Based Thermal Imagery to Detect Crop Water Status Variability in Cotton. *Smart Agric. Technol.* **2022**, *2*, 100029. [CrossRef]
2. Sepulcre-Cantó, G.; Zarco-Tejada, P.J.; Jiménez-Muñoz, J.C.; Sobrino, J.A.; Miguel, E.d.; Villalobos, F.J. Detection of Water Stress in an Olive Orchard with Thermal Remote Sensing Imagery. *Agric. For. Meteorol.* **2006**, *136*, 31–44. [CrossRef]
3. Jones, H.G. Irrigation Scheduling: Advantages and Pitfalls of Plant-Based Methods. *J. Exp. Bot.* **2004**, *55*, 2427–2436. [CrossRef] [PubMed]
4. Zhang, Y.; Han, W.; Zhang, H.; Niu, X.; Shao, G. Evaluating Soil Moisture Content Under Maize Coverage Using UAV Multimodal Data by Machine Learning Algorithms. *J. Hydrol.* **2023**, *617*, 129086. [CrossRef]
5. Bertalan, L.; Holb, I.; Pataki, A.; Négyesi, G.; Szabó, G.; Szalóki, A.K.; Szabó, S. UAV-Based Multispectral And Thermal Cameras to Predict Soil Water Content—A Machine Learning Approach. *Comput. Electron. Agric.* **2022**, *200*, 107262. [CrossRef]
6. Zhu, H.; Huang, Y.; An, Z.; Zhang, H.; Han, Y.; Zhao, Z.; Li, F.; Zhang, C.; Hou, C. Assessing Radiometric Calibration Methods for Multispectral UAV Imagery And The Influence of Illumination, Flight Altitude And Flight Time on Reflectance, Vegetation Index And Inversion of Winter Wheat AGB And LAI. *Comput. Electron. Agric.* **2024**, *219*, 108821. [CrossRef]
7. Guo, F.; Feng, Q.; Yang, S.; Yang, W. Estimation of Potato Canopy Leaf Water Content in Various Growth Stages Using UAV Hyperspectral Remote Sensing And Machine Learning. *Front. Plant Sci.* **2024**, *15*, 1458589. [CrossRef]
8. Chen, S.; Chen, Y.; Chen, J.; Zhang, Z.; Ma, Y. Retrieval of Cotton Plant Water Content by UAV-Based Vegetation Supply Water Index (VSWI). *Int. J. Remote Sens.* **2020**, *41*, 4389–4407. [CrossRef]
9. Zhou, X.; Zheng, H.B.; Xu, X.Q.; He, J.Y.; Ge, X.K.; Yao, X.; Cheng, T.; Zhu, Y.; Cao, W.X.; Tian, Y.C. Predicting Grain Yield in Rice Using Multi-Temporal Vegetation Indices from UAV-Based Multispectral and Digital Imagery. *ISPRS J. Photogramm. Remote Sens.* **2017**, *130*, 246–255. [CrossRef]

10. Wang, C.; Zhu, K.; Bai, Y.; Li, C.; Li, M.; Sun, Y. Response of Stomatal Conductance to Plant Water Stress in Buffalograss Seed Production: Observation with UAV Thermal Infrared Imagery. *Agr. Water Manag.* **2024**, *292*, 108661. [CrossRef]
11. Lu, J.; Wu, Y.; Liu, H.; Gou, T.; Zhao, S.; Chen, F.; Jiang, J.; Chen, S.; Fang, W.; Guan, Z. Estimation of Plant Water Content in Cut Chrysanthemum Using Leaf-Based Hyperspectral Reflectance. *Sci. Hortic.* **2024**, *323*, 112517. [CrossRef]
12. Zhang, F.; Zhou, G. Estimation of Vegetation Water Content Using Hyperspectral Vegetation Indices: A Comparison of Crop Water Indicators in Response to Water Stress Treatments for Summer Maize. *BMC Ecol.* **2019**, *19*, 18. [CrossRef]
13. Pei, S.; Dai, Y.; Bai, Z.; Li, Z.; Zhang, F.; Yin, F.; Fan, J. Improved Estimation of Canopy Water Status in Cotton Using Vegetation Indices Along with Textural Information from UAV-Based Multispectral Images. *Comput. Electron. Agric.* **2024**, *224*, 109176. [CrossRef]
14. Zhou, Y.; Lao, C.; Yang, Y.; Zhang, Z.; Chen, H.; Chen, Y.; Chen, J.; Ning, J.; Yang, N. Diagnosis of Winter-Wheat Water Stress Based on UAV-Borne Multispectral Image Texture and Vegetation Indices. *Agric. Water Manag.* **2021**, *256*, 107076. [CrossRef]
15. Santesteban, L.G.; Di Gennaro, S.F.; Herrero-Langreo, A.; Miranda, C.; Royo, J.B.; Matese, A. High-Resolution UAV-Based Thermal Imaging to Estimate The Instantaneous And Seasonal Variability of Plant Water Status within A Vineyard. *Agric. Water Manag.* **2017**, *183*, 49–59. [CrossRef]
16. Morales-Santos, A.; Nolz, R. Assessment of Canopy Temperature-Based Water Stress Indices for Irrigated And Rainfed Soybeans Under Subhumid Conditions. *Agric. Water Manag.* **2023**, *279*, 108214. [CrossRef]
17. DeJonge, K.C.; Taghvaeian, S.; Trout, T.J.; Comas, L.H. Comparison of Canopy Temperature-Based Water Stress Indices for Maize. *Agr. Water Manag.* **2015**, *156*, 51–62. [CrossRef]
18. Tuia, D.; Volpi, M.; Copa, L.; Kanevski, M.; Muñoz-Marí, J. A Survey of Active Learning Algorithms for Supervised Remote Sensing Image Classification. *IEEE J. Stsp* **2011**, *5*, 606–617. [CrossRef]
19. Mutanga, O.; Adam, E.; Cho, M.A. High Density Biomass Estimation for Wetland Vegetation Using WorldView-2 Imagery And Random Forest Regression Algorithm. *Int. J. Appl. Earth Obs.* **2012**, *18*, 399–406. [CrossRef]
20. Foody, G.M.; Mathur, A. A Relative Evaluation of Multiclass Image Classification by Support Vector Machines. *IEEE Trans. Geosci. Remote Sens.* **2004**, *42*, 1335–1343. [CrossRef]
21. Peng, X.L.; Ma, Y.X.; Sun, J.; Chen, D.Y.; Zhen, J.B.; Zhang, Z.T.; Hu, X.T.; Wang, Y.K. Grape Leaf Moisture Prediction from UAVs Using Multimodal Data Fusion And Machine Learning. *Precis. Agric.* **2024**, *25*, 1609–1635. [CrossRef]
22. Dong, H.; Dong, J.; Sun, S.; Bai, T.; Zhao, D.; Yin, Y.; Shen, X.; Wang, Y.; Zhang, Z.; Wang, Y. Crop Water Stress Detection Based on UAV Remote Sensing Systems. *Agric. Water Manag.* **2024**, *303*, 109059. [CrossRef]
23. Tucker, C.J. Red and Photographic Infrared Linear Combinations for Monitoring Vegetation. *Remote Sens. Environ.* **1979**, *8*, 127–150. [CrossRef]
24. Candiago, S.; Remondino, F.; De Giglio, M.; Dubbini, M.; Gattelli, M. Evaluating Multispectral Images and Vegetation Indices for Precision Farming Applications from UAV Images. *Remote Sens.* **2015**, *7*, 4026–4047. [CrossRef]
25. Steven, M.D. The Sensitivity of The OSAVI Vegetation Index to Observational Parameters. *Remote Sens. Environ.* **1998**, *63*, 49–60. [CrossRef]
26. Hatfield, J.L.; Prueger, J.H. Value of Using Different Vegetative Indices to Quantify Agricultural Crop Characteristics at Different Growth Stages under Varying Management Practices. *Remote Sens.* **2010**, *2*, 562–578. [CrossRef]
27. Qi, J.; Chehbouni, A.; Huete, A.R.; Kerr, Y.H.; Sorooshian, S. A Modified Soil Adjusted Vegetation Index. *Remote Sens. Environ.* **1994**. [CrossRef]
28. Broge, N.H.; Mortensen, J.V. Deriving Green Crop Area Index And Canopy Chlorophyll Density of Winter Wheat from Spectral Reflectance Data. *Remote Sens. Environ.* **2002**, *81*, 45–57. [CrossRef]
29. Hassan, M.A.; Yang, M.J.; Rasheed, A.; Jin, X.L.; Xia, X.C.; Xiao, Y.G.; He, Z.H. Time-Series Multispectral Indices from Unmanned Aerial Vehicle Imagery Reveal Senescence Rate in Bread Wheat. *Remote Sens.* **2018**, *10*, 809. [CrossRef]
30. Gitelson, A.A.; Viña, A.; Ciganda, V.; Rundquist, D.C.; Arkebauer, T.J. Remote Estimation of Canopy Chlorophyll Content in Crops. *Geophys. Res. Lett.* **2005**, *32*, L08403. [CrossRef]
31. Maes, W.H.; Steppe, K. Perspectives for Remote Sensing with Unmanned Aerial Vehicles in Precision Agriculture. *Trends Plant Sci.* **2019**, *24*, 152–164. [CrossRef] [PubMed]
32. Potgieter, A.B.; George-Jaeggli, B.; Chapman, S.C.; Laws, K.; Suarez Cadavid, L.A.; Wixted, J.; Watson, J.; Eldridge, M.; Jordan, D.R.; Hammer, G.L. Multi-Spectral Imaging from an Unmanned Aerial Vehicle Enables the Assessment of Seasonal Leaf Area Dynamics of Sorghum Breeding Lines. *Front. Plant Sci.* **2017**, *8*, 1532. [CrossRef]
33. Ballester, C.; Hornbuckle, J.; Brinkhoff, J.; Smith, J.; Quayle, W. Assessment of In-Season Cotton Nitrogen Status And Lint Yield Prediction from Unmanned Aerial System Imagery. *Remote Sens.* **2017**, *9*, 1149. [CrossRef]
34. Dempewolf, J.; Adusei, B.; Becker-Reshef, I.; Hansen, M.; Potapov, P.; Khan, A.; Barker, B. Wheat Yield Forecasting for Punjab Province from Vegetation Index Time Series and Historic Crop Statistics. *Remote Sens.* **2014**, *6*, 9653–9675. [CrossRef]
35. Apan, A.; Held, A.; Phinn, S.; Markley, J. Detecting Sugarcane 'Orange Rust' Disease Using EO-1 Hyperion Hyperspectral Imagery. *Int. J. Remote Sens.* **2004**, *25*, 489–498. [CrossRef]

36. Penuelas, J.; Baret, F.; Filella, I. Semiempirical Indexes to Assess Carotenoids Chlorophyll-A Ratio from Leaf Spectral Reflectance. *Photosynthetica* **1995**, *31*, 221–230. [CrossRef]
37. Tanner, C.B. Plant Temperatures. *Agron. J.* **1963**, *55*, 210–211. [CrossRef]
38. Cao, Q.; Miao, Y.X.; Wang, H.Y.; Huang, S.Y.; Cheng, S.S.; Khosla, R.; Jiang, R.F. Non-Destructive Estimation of Rice Plant Nitrogen Status with Crop Circle Multispectral Active Canopy Sensor. *Field Crop Res.* **2013**, *154*, 133–144. [CrossRef]
39. Elsayed, S.; Rischbeck, P.; Schmidhalter, U. Comparing the Performance of Active And Passive Reflectance Sensors to Assess The Normalized Relative Canopy Temperature And Grain Yield of Drought-Stressed Barley Cultivars. *Field Crop Res.* **2015**, *177*, 148–160. [CrossRef]
40. Abdi, H. Partial Least Squares Regression And Projection on Latent Structure Regression (PLS-Regression). *WIREs. Comput. Stat.* **2010**, *2*, 97–106. [CrossRef]
41. Smola, A.J.; Schölkopf, B. A Tutorial on Support Vector Regression. *Stat. Comput.* **2004**, *14*, 199–222. [CrossRef]
42. Breiman, L. Random Forests. *Mach. Learn.* **2001**, *45*, 5–32. [CrossRef]
43. Chen, T.; Guestrin, C. XGBoost: A Scalable Tree Boosting System. In Proceedings of the 22nd ACM SIGKDD International Conference on Knowledge Discovery and Data Mining, San Francisco, CA, USA, 13–17 August 2016; pp. 5–32. [CrossRef]
44. Fan, J.; Zheng, J.; Wu, L.; Zhang, F. Estimation of Daily Maize Transpiration Using Support Vector Machines, Extreme Gradient Boosting, Artificial And Deep Neural Networks Models. *Agric. Water Manag.* **2021**, *245*, 106547. [CrossRef]
45. Bowyer, P.; Danson, F.M. Sensitivity of Spectral Reflectance to Variation in Live Fuel Moisture Content at Leaf And Canopy Level. *Remote Sens. Environ.* **2004**, *92*, 297–308. [CrossRef]
46. Wang, J.; Lou, Y.; Wang, W.; Liu, S.; Zhang, H.; Hui, X.; Wang, Y.; Yan, H.; Maes, W.H. A Robust Model for Diagnosing Water Stress of Winter Wheat by Combining UAV Multispectral And Thermal Remote Sensing. *Agric. Water Manag.* **2024**, *291*. [CrossRef]
47. Basinger, N.T.; Jennings, K.M.; Hestir, E.L.; Monks, D.W.; Jordan, D.L.; Everman, W.J. Phenology Affects Differentiation of Crop And Weed Species Using Hyperspectral Remote Sensing. *Weed Technol.* **2020**, *34*, 897–908. [CrossRef]
48. Fan, Y.; Liu, J.; Zhao, J.; Ma, Y.; Li, Q. Effects of Delayed Irrigation during The Jointing Stage on The Photosynthetic Characteristics And Yield of Winter Wheat under Different Planting Patterns. *Agric. Water Manag.* **2019**, *221*, 371–376. [CrossRef]
49. Yu, J.-W.; Yoon, Y.-W.; Baek, W.-K.; Jung, H.-S. Forest Vertical Structure Mapping Using Two-Seasonal Optic Images and LiDAR DSM Acquired from UAV Platform through Random Forest, XGBoost, and Support Vector Machine Approaches. *Remote Sens.* **2021**, *13*, 4282. [CrossRef]
50. Rashid, M.; Bari, B.S.; Yusup, Y.; Kamaruddin, M.A.; Khan, N. A Comprehensive Review of Crop Yield Prediction Using Machine Learning Approaches With Special Emphasis on Palm Oil Yield Prediction. *IEEE Access* **2021**, *9*, 63406–63439. [CrossRef]
51. Thenkabail, P.S.; Smith, R.B.; De Pauw, E. Hyperspectral Vegetation Indices And Their Relationships with Agricultural Crop Characteristics. *Remote Sens. Environ.* **2000**, *71*, 158–182. [CrossRef]
52. Meerdink, S.; Roberts, D.; Hulley, G.; Gader, P.; Pisek, J.; Adamson, K.; King, J.; Hook, S.J. Plant Species' Spectral Emissivity And Temperature Using The Hyperspectral Thermal Emission Spectrometer (HyTES) Sensor. *Remote Sens. Environ.* **2019**, *224*, 421–435. [CrossRef]
53. Yang, N.; Zhang, Z.; Ding, B.; Wang, T.; Zhang, J.; Liu, C.; Zhang, Q.; Zuo, X.; Chen, J.; Cui, N.; et al. Evaluation of Winter-Wheat Water Stress with UAV-Based Multispectral Data And Ensemble Learning Method. *Plant Soil* **2024**, *497*, 647–668. [CrossRef]